Systematic Investigation of Porogen Size and Content on Scaffold Morphometric Parameters and Properties

Sheng Lin-Gibson,* James A. Cooper, Forrest A. Landis,† and Marcus T. Cicerone

Polymers Division, National Institute of Standards and Technology, Gaithersburg, Maryland 20899-8543

Received December 1, 2006; Revised Manuscript Received February 2, 2007

A systematic investigation of tissue engineering scaffolds prepared by salt leaching of a photopolymerized dimethacrylate was performed to determine how the scaffold structure (porosity, pore size, etc.) can be controlled and also to determine how the scaffold structure and the mechanical properties are related. Two series of scaffolds were prepared with (1) the same polymer-to-salt ratio but different salt sizes (ranging from average size of 100 to 390 μm) and (2) the same salt size but different polymer-to-salt ratios (ranging from salt mass of 70 to 90%). These scaffolds were examined to determine how the fabrication parameters affected the scaffold morphometric parameters and corresponding mechanical properties. Combined techniques of X-ray microcomputed tomography (μCT), mercury porosimetry, and gravimetric analysis were used to determine the scaffold parameters, such as porosity, pore size, and strut thickness and their size distributions, and pore interconnectivity. Scaffolds with porosities ranging from 57% to 92% (by volume) with interconnected structures could be fabricated using the current technique. The porosity and strut thickness were subsequently related to the mechanical response of the scaffolds, both of which contribute to the compression modulus of the scaffold. The current study shows that the structure and properties of the scaffold could be tailored by the size and the amount of porogen used in the fabrication of the scaffold.

Introduction

Tissue engineering approaches are currently being extensively investigated because they hold the promise for regenerating or replacing damage tissues. One tissue engineering approach for bone therapy involves the use of porous, polymeric scaffolds which serve as the mechanical framework to which cells attach and proliferate. In an ideal situation, the scaffold should slowly degrade to benign products over time within the organism leaving regenerated, self-supporting tissue. Many different techniques have been developed to fabricate scaffolds for these applications, including methods that generate precisely controlled geometries such as fused deposition modeling, 3D printing, and stereolithography,[1,2] and methods that use porogens, phase separation, gas foaming,[3] or supercritical fluid[4] to form less ordered pore structures. A significant effort has been devoted to the design and fabrication of scaffolds to optimize their performance with respect to in-vivo or in-vitro growth conditions.[5]

We and others have used salt-leached photopolymerizable polymers as a means for producing porous scaffolds for tissue engineering applications.[6−9] Advantages of the photopolymerized salt-leaching process include a relatively easy fabrication procedure, absence of toxic solvent, and the ability to tailor the mechanical properties and scaffold architectures to meet specific applications. Currently, we are using a model scaffold system based on photopolymerized ethoxylated *bis*-phenol A dimethacrylates (EBPADMA) for investigating several structure−functional−biological properties. This and similar dimethacrylate materials have found extensive use in a variety of dental applications. In addition to aforementioned desirable properties, these photopolymerized scaffolds are ideal for visible and near-infrared light in optical microscopies (e.g., they have no crystallinity which minimizes scattering, they exhibit essentially no autofluorescence, and they do not adsorb common cell stains). They also have been shown to promote good cell adhesion and growth and can be hydrolytically stable over several weeks in cell growth media.[7] The latter property is an important factor for long-term in-vitro studies of cell penetration and proliferation.

Regardless of the fabrication method used, the scaffold structure can be described by morphometric parameters (e.g., porosity, pore size, strut thickness, surface-area-to-volume ratio, and interconnectivity).[10,11] These and other characteristics (such as mechanical properties and biocompatibility) determine the performance of scaffolds.[5] For example, scaffolds prepared with a high porosity and high surface-area-to-volume ratios (small pores) are important for cell seeding and attachment. In contrast, larger pore sizes have been shown to favor osteogenesis. It is often difficult to optimize a specific parameter without sacrificing the performance of another property. For example, a scaffold containing the desired high porosity is likely to exhibit weak mechanical strength and modulus. These structural parameters also affect the interconnectivity and permeability of the scaffold, which in turn, affect the transport properties.[12]

The scaffold structure is expected to dictate the corresponding mechanical properties. Relationships between the structure of foams (cellular solids) and mechanical properties have been the subject of extensive experimental and theoretical research.[13] Tissue engineering scaffolds, which have similar structural characteristics to polymeric foams, have also been examined to determine the relationship between structures (porosity and pore size) and mechanical properties. The general trend is that the mechanical properties (e.g., compression modulus and rigidity) will increase with a decrease in the porosity.[8,14−16] Photopolymerized poly(propylene fumarate) scaffolds with 80

* To whom correspondence should be addressed. E-mail: slgibson@nist.gov.

† Current address: Department of Chemistry, Penn State York, York, PA 17403.

10.1021/bm061139q CCC: $37.00
Published on Web 03/24/2007

mass % porogen[8] possessed an interconnected pore structure and superior mechanical properties compared to typical polyester scaffolds. It has been reported that low-porosity scaffolds (35−40%) fabricated by sintering poly(lactide-*co*-glycolide) microspheres showed that an increase in the pore size resulted in a modest decrease in compressive modulus.[17] While several general trends are available, a systematic investigation into how the morphometric parameters, particularly how a large distribution of pore sizes and strut thicknesses, affect the mechanical properties of a polymeric scaffold is still lacking.

The morphometric parameters and mechanical properties cannot be predicted a priori for scaffolds generated by the salt-leaching process and must be characterized. Methods for determining the scaffold morphometric parameters include scanning electron microscopy (SEM), mercury porosimetry, and X-ray microcomputed tomography (μCT).[10] In addition, theories are well-established for estimating the mechanical properties of foam materials with well-defined pore and strut structures but have not been used to evaluate their application for tissue engineering scaffolds. Although the salt-leaching process leads to imprecise scaffold mesostructures, it is still possible to achieve significant control over various morphometric parameters and mechanical properties. Processing parameters for controlling these properties must be determined. A better understanding of how the scaffold structure generated by the salt-leaching process affects the mechanical properties is needed. These are two areas which we will attempt to address.

In this study, we prepare a series of photopolymerized dimethacrylate scaffolds with sodium chloride as the porogen. By varying the size of the salt porogen and the polymer-to-salt ratio, we show that it is possible to quantitatively control not only the scaffold morphometric parameters but also the mechanical properties. We examine how the scaffold structure and properties can be controlled by the fabrication process and how scaffold structure relates to the mechanical properties. The scaffold morphology is examined using complimentary characterization techniques including gravimetric analysis, mercury porosimetry, and μCT analysis, and the mechanical properties of the scaffolds are determined using compression tests. The scaffold porosity, pore size, strut thickness distributions, interconnectivity, and compressive properties are determined and correlated.

Experimental

Ethoxylated bisphenol A dimethacrylate (EBPADMA, degree of ethoxylation $\approx$ 6) was obtained from Esstech Inc. The photoinitiator system of camphorquinone (CQ) and ethyl 4-*N*,*N*-dimethylaminobenzoate (4E) was purchased from Aldrich Corp. All reagents were used as received. The resin was activated with a redox photoinitiator system consisting of 0.2% CQ and 0.8% 4E (by mass) and was stored in the dark until use. Sodium chloride crystals (from Mallinckrodt Baker, Inc.) were ground into smaller particles using a mortar and pestle and then were separated into defined size ranges using brass sieves (Fisher Scientific, Inc.) with nominal sieve openings of 425, 355, 250, 150, and 75 μm. The midpoint of the range between the sieve openings was taken as the average size of the salt crystals (i.e., a 250-μm sieve and a 150-μm sieve yield an average porogen size of 200 μm).

Fabrication of EBPADMA Tissue Engineering Scaffolds. Scaffolds were prepared using procedures that have been described in detail elsewhere.[7] The specific sample geometry was chosen to accommodate multiple physical and biological studies. Briefly, activated EBPADMA was blended with sieved salt crystals in the appropriate mass ratios. With the exception of the 30% resin mixture, all mixtures were packed into a polytetrafluoroethylene (PTFE) frame mold (3-mm thick) with 9-mm-diameter clear bore holes. The frame was pressed together between two glass plates and was cured for 5 min per side in a Dentsply Triad 2000 visible light cure unit with a tungsten halogen light bulb (250 W and 120 V). The slurry containing 30% resin was too fluid to be used in the PTFE frame and instead was poured into a 9-mm-diameter round PTFE mold bored out to a depth of 3 mm. The mold was covered with a piece of plastic film and was cured for 5 min from the top side of the scaffold. The scaffold was then removed from the mold and the bottom side of the scaffold was cured for an additional 5 min. After irradiation, all samples were postcured in a vacuum oven at 100 °C for 1 h. The circular composite samples were soaked in deionized water for 5 days with several changes of the water to dissolve the salt porogen and to leave a porous scaffold. Treatment of the water with a silver nitrate solution after 5 days showed no evidence of AgCl precipitate indicating that the water-accessible salt had been removed from scaffolds.

Porosity Calculation. In the current study, we calculated a targeted porosity on the basis of the polymer-to-salt mass ratio used in the formulation and experimentally determined the porosity on the basis of the mass loss (gravimetric analysis), by μCT analysis, and in some cases by mercury porosimetry. Using densities of 2.165 g/cm^3 and 1.198 g/cm^3 for the salt and polymerized EBPADMA, respectively, the targeted porosity of the scaffold was calculated for each sample using eq 1[18]

$$\text{targeted porosity} = \frac{M_{\text{resin}}/1.198}{(M_{\text{resin}}/1.198 + M_{\text{salt}}/2.165)} \times 100 \quad (1)$$

where the M_{resin} and M_{salt} are the initial measured mass of the resin and salt, respectively. The actual porosity was determined using the above equation by replacing M_{resin} with the final mass of the soaked scaffold. The porosity of the samples was determined using gravimetric analysis of the average mass loss of five samples after the soaking process.

X-ray Microcomputed Tomography (μCT). The internal morphology of the scaffolds was characterized using a Scanco μCT 40 instrument. The microfocus X-ray source was set at 45 kVp and 177 μA to give a spot size of 5 μm. The samples were scanned at an 8-μm voxel resolution with an integration time of 300 s. Three specimens were scanned for each sample type. After completion of the *xy* scans, 100−300 slices were reconstructed and analyzed using the manufacturer's complete imaging and evaluation solution software. The segmentation values were chosen and kept constant for samples with a constant polymer-to-salt ratio; however, it was necessary to adjust the segmentation for the series of scaffolds prepared with varying salt contents to achieve the optimal binary pore-solid space. A component labeling procedure was applied to all images to remove disconnected pieces. Morphometric parameters, including porosity, pore size, and strut thickness, were calculated using direct distance transformation methods developed by Hilderbrand and Ruegsegger.[19] The 3D renderings illustrated are of a small section of the scaffolds; however, results shown are calculated from the entire scaffold volume.

Mercury Porosimetry. Mercury porosimetry is an established method used to study microporous matrixes that use the Washburn equation relating pressure to the size of the intruded pore diameter,[20] $DP = -4\gamma \cos \theta$, where D represents pore diameter, P is applied pressure, γ is surface tension, and θ is the contact angle between mercury and pore wall (130° at ambient temperature). The scaffolds were examined with a porosimeter (Micromeritics Autopore III, GA) using low-pressure ports with a maximum intrusion pressure of 40 psi. The pressure on the system is increased in incremental steps to allow for mercury intrusion. By measuring the intruded volume at each step until the maximum pressure is reached, the porosity of the system can be determined. After testing the samples, analysis of porosity, pore surface area, and pore diameter distribution were evaluated. Three specimens were run for each sample and the porosity is reported with one standard deviation of uncertainty.

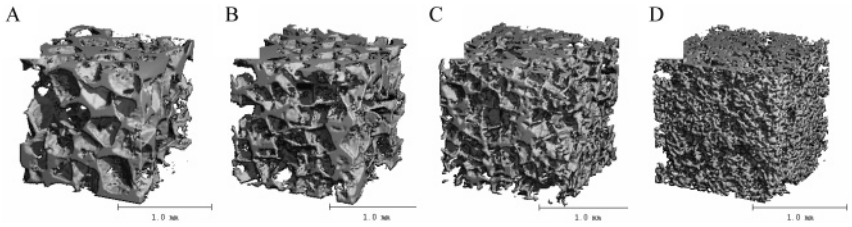

Figure 1. 3D renderings from μCT analysis of scaffolds prepared with a constant polymer-to-salt ratio but varying salt crystal sizes: (A) DMA-74p-100, (B) DMA-74p-200, (C) DMA-74p-300, and (D) DMA-74p-390. Each cube represents a volume of 1.7 mm^3.

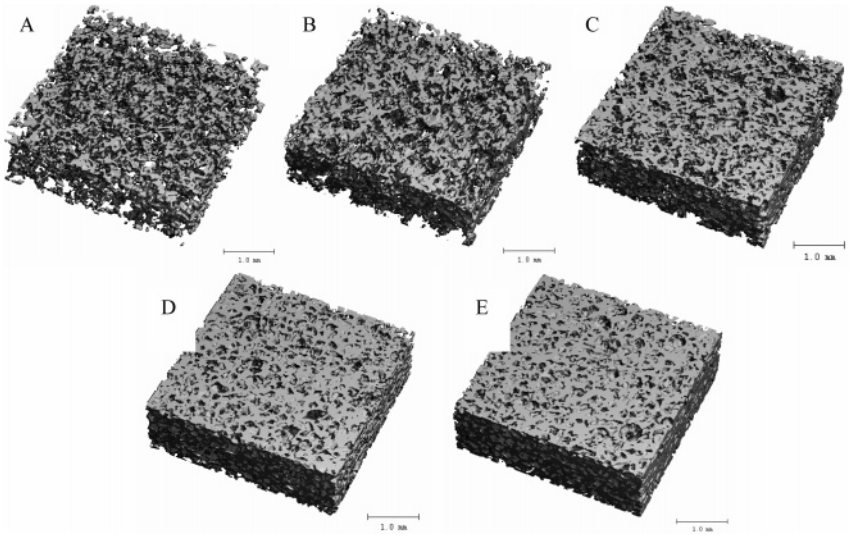

Figure 2. 3D renderings from μCT analysis of scaffolds prepared with varying 200-μm salt contents: (A) DMA-83p-200, (B) DMA-76p-200, (C) DMA-69p-200, (D) DMA-62p-200, and (E) DMA-56p-200. Each cube represents a volume of 15 mm^3.

Mechanical Measurements. The compressive strength of the scaffolds was determined using an RSA III dynamic mechanical analyzer (TA Instruments) with a 3500-g load cell. The disc-shaped samples (approximately 9 mm in diameter by 3 mm in height) were compressed at a rate of 50 μm/s. The compressive strength and modulus of the samples were calculated in a manner similar to ASTM method D 1621-04a.[21] While the aspect ratio for the samples measured is within the recommended range, previous work has shown that the aspect ratio affects the failure behavior.[22] The samples measured in the current study have a low aspect ratio which gives a more stable compression while reducing some shear stress effects. The reported compression moduli were an average of five samples for each pore size and were reported with one standard deviation of uncertainty. The mode of deformation is complex and likely involves the buckling of struts.

Results and Discussion

We show results for two series of photopolymerized scaffolds, one series prepared by changing the average porogen size from 100 to 390 μm at a near constant pore volume fraction and one series prepared with varying pore volume fraction using a 200-μm-size porogen. Throughout the rest of the article, we will refer to the samples as DMA-*x*p-*y* where is *x* is the % porosity on the basis of the formulation calculated using eq 1, and *y* is the mean porogen size (e.g., DMA-74p-300 would be a scaffold prepared with a targeted porosity of 74% and salt crystals of an average size of 300 μm).

The first series consists of four scaffolds prepared with average crystal sizes of 390, 300, 200, and 100 μm and a constant polymer-to-salt ratio with a targeted porosity of 74% (Figure 1). The 3D renderings from μCT analysis clearly illustrate an increase in the scaffold pore sizes as the average salt crystal size increased from 100 to 390 μm. At a constant porosity, the porogen size dictates the scaffold pore size and pore size distribution. In addition, the pores became more rectilinear as the pore size increased because of the cubic shape of the larger salt crystals.

Table 1. Porosity of Scaffolds Prepared from Varying Polymer-to-Salt Ratios

polymer mass %	salt mass %	porosity %
10	90	83
15	85	76
20	80	69
25	75	62
30	70	56

Table 2. Comparison of Porosity Determined by μCT, Gravimetric Analysis, and Hg Porosimetry[a]

average porogen size (μm)	μCT %	gravimetric %	Hg porosimetry %
100	76.8 $\pm$ 4.0	81.5 $\pm$ 1.5	78.8 $\pm$ 1.2
200	78.0 $\pm$ 2.6	78.0 $\pm$ 1.5	79.8 $\pm$ 3.8
300	76.3 $\pm$ 1.5	75.2 $\pm$ 0.8	74.3 $\pm$ 5.4
390	77.0 $\pm$ 1.5	73.4 $\pm$ 1.2	64.7 $\pm$ 7.6

[a] The targeted porosity based on the formulation is 74%.

The second series consists of five scaffolds prepared from mixtures of dimethacrylate and 200-μm salt crystals with the porogen content ranging from 70% to 90% (by mass) in 5% increments. The corresponding porosities calculated on the basis of the formulation using the density of the salt and polymer are listed in Table 1. As expected, the 3D renderings show that the scaffolds became denser as the polymer content was increased (Figure 2). For scaffolds prepared with the same size porogen, the pore size and structure is governed by the tendency of the

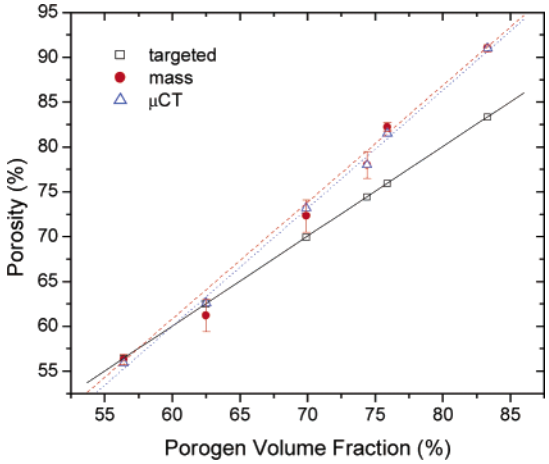

Figure 3. A comparison of the porosity obtained from gravimetric and μCT analysis of the scaffolds prepared from 200-μm salt crystals with varying mass % of polymer. The lines are linear fits of each data set.

salt crystals to form contact points. The more contact points that exist between the salt crystals, the larger the average pore size would be. By increasing the amount of polymer in the formulation, less contact between salt crystals can occur.

Porosity. Table 2 compares the porosity values for the series of scaffolds prepared with varying porogen size (theoretical porosity = 74%) obtained by gravimetric analysis, μCT, and mercury porosimetry. Results obtained via the three experimental methods agreed well for scaffolds prepared with the two intermediate salt crystal sizes (200 and 300 μm). Gravimetric analysis yielded a slightly higher porosity for the scaffolds prepared with the smallest salt crystal size (100 μm) compared to those calculated by other techniques. This scaffold had thin struts and is less robust; therefore, small sections of polymer lost from the scaffold surface during the 5-day soaking process would lead to a higher apparent porosity. On the other hand, mercury porosimetry grossly underestimated the porosity of the scaffold made with largest salt crystal size. The mercury porosimeter we used operates best in the regions below approximately 300 μm. The large pore scaffolds are beyond that size, and the instrument is operating at the limits of its range. While the μCT provided relatively consistent values for the porosity, analysis depended on the segmentation values chosen by the operator and errors arise from the segmentation values that increased as the strut thickness decreased.

Figure 3 shows the porosity of scaffolds prepared with varying polymer-to-salt ratios calculated from the formulation composition and measured by gravimetric and μCT analysis. Data from the 74% scaffold (from the first series of scaffolds) are also included. The porosity determined by gravimetric analysis and μCT agreed very well. However, an increasing deviation in the porosity value from the targeted value was observed for scaffolds prepared with increasing porosity above 60%. The reason for this discrepancy is likely due to insufficient wetting of the salt crystals during fabrication at the lower polymer contents, which would result in unconnected polymer particles and would lead to a higher than expected porosity.

Pore Size and Strut Thickness and Their Distributions. Figure 4 demonstrates the relationship between the pore size and strut thickness computed from the μCT images shown in Figure 1. The data quantitatively show that both the pore size and strut thickness increased as the porogen size increased. In addition, the distributions of the pore size and strut thickness became broader as the salt crystal size increased. The distance transformation algorithm used in describing the current scaffolds with irregular pore shapes, high interconnectivity, and high tortuosity is expected to produce broad distributions. We expect a significant portion of the smaller pores to be channels that connect the larger domains. Samples prepared with porogens of average size 100, 200, and 300 μm had pore size distributions that ranged from 8 μm (a single voxel) to the upper size limit of the porogen. The sample prepared with the largest porogen (average size is 390 μm, upper size limit of 425 μm) showed a broader pore size distribution ranging from 8 to 680 μm. As

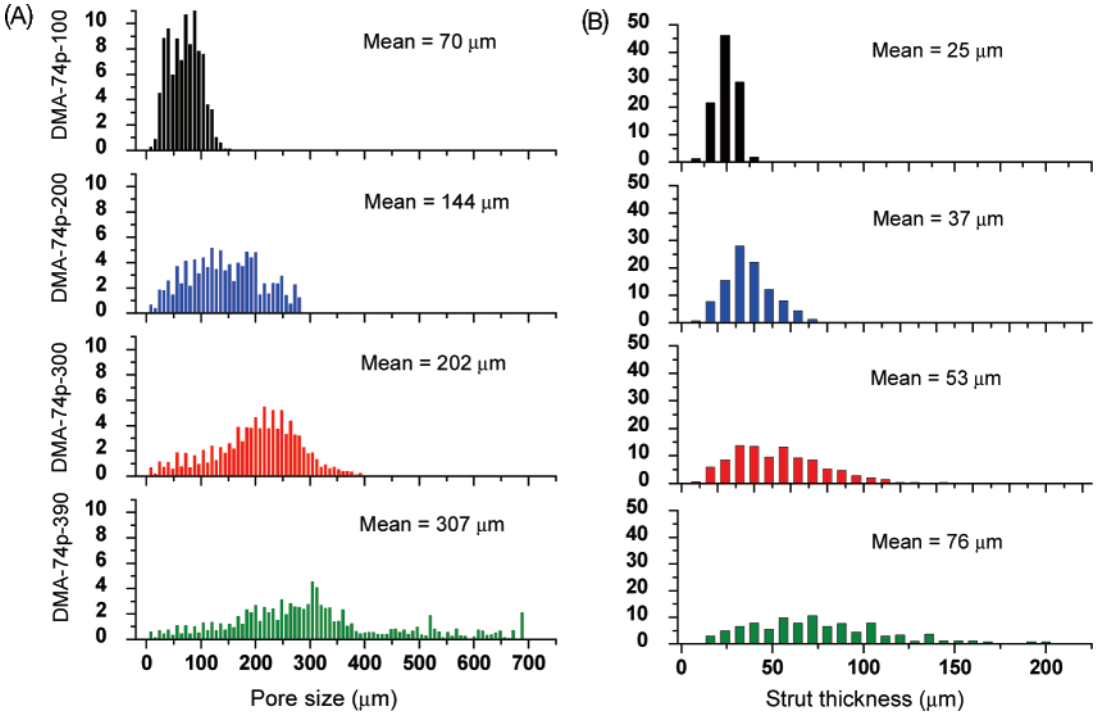

Figure 4. Analysis of (A) pore size and (B) strut thickness from the 3D X-ray μCT images of scaffolds prepared with a constant polymer-to-salt ratio but varying salt crystal sizes.

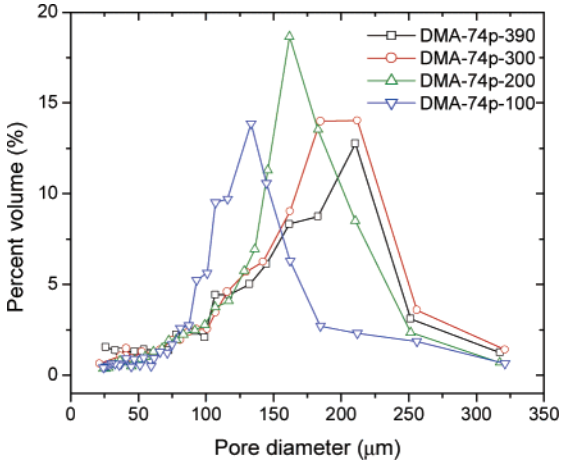

Figure 5. Mercury porosimetry analysis of scaffolds prepared with a constant polymer-to-salt ratio but varying salt crystal sizes. The error bars have been omitted for clarity.

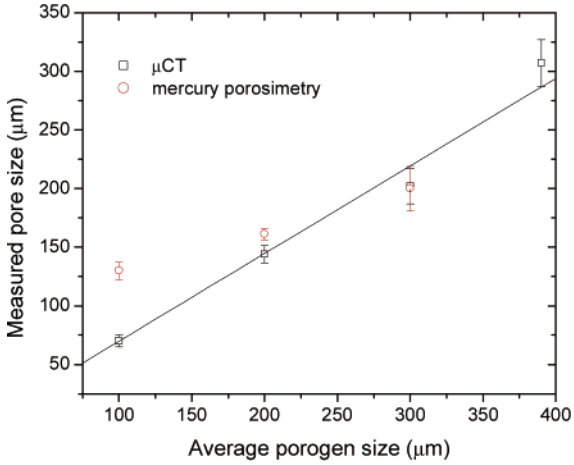

Figure 6. Comparison of the average pore sizes obtained from μCT and mode pore sizes obtained from mercury porosimetry with the average porogen size. The line represents a linear fit of the μCT data.

indicated by the histogram, a significant amount of pore volume had a larger size than the largest porogen size. The pore size is directly related to the strut thickness for scaffolds with a near identical porosity. As the pore size decreases, a larger number of pores must exist to maintain a constant porosity; therefore, the average strut thickness must also decrease. Moreover, the surface-area-to-volume ratio would increase with small pores. Larger pores (>100 μm) promote osteogenesis and allow vascularization; however, very large pores can reduce the surface area for cells and slow down cell proliferation.[5] Therefore, the optimization of pore size is crucial in microporous matrixes to be seeded with cells. These results indicate that all scaffolds had pore sizes suitable for bone tissue formation as larger pores have been demonstrated to be necessary for osteogenesis and small pores will increase the surface-area-to-volume ratio.

We also conducted mercury porosimetry analysis to determine the pore size, pore size distribution, and surface area for scaffolds prepared with varying porogen sizes. The percent pore volume of the scaffolds versus the measured pore diameter is plotted in Figure 5. Each composition was measured three times, and the average is shown. The curves for scaffolds prepared using the smaller salt sizes were symmetrical and appear to describe the entire pore size distribution; however, the curves for the scaffolds prepared with larger salt sizes, particularly the 390-μm salt crystals, were less symmetrical and appear to only capture the smaller pore sizes instead of the entire pore size distribution. Results showed the expected trend of increased pore size with increased porogen size, consistent with the μCT analysis.

The pore sizes obtained from μCT and mercury porosimetry were compared to that of the average porogen size, and the results are shown in Figure 6. The value for the scaffold prepared with the 390-μm porogen measured by mercury porosimetry was omitted. A near linear relationship between the average pore size obtained by μCT and the average porogen size was observed. In addition, results obtained by the two experimental methods agreed very well for scaffolds prepared with the two intermediate salt sizes. As noted previously, the porosity values for these two scaffolds also agreed very well. The pore size obtained from μCT deviated significantly from that obtained using mercury porosimetry for scaffolds fabricated using the smallest salt sizes.

A similar analysis on pore size and strut thickness was carried out on the second series of scaffolds. The histograms describing the pore size and strut thickness distribution are shown in Figure 7. The overall trend is that the average pore size decreased and the average strut thickness increased as the polymer content increased. This is in contrast to the first series of scaffolds where both the pore size and strut thickness increased concurrently. In addition, the pore size distribution increased with decreased polymer concentration, but the strut thickness distribution did not change significantly. A near monotonic shift toward higher values was observed for the strut thickness as the salt content was decreased from 90% to 70% (by mass). For compositions low in porogen content, changes in the pore size distribution were relatively small. It appears that at those compositions, increasing the polymer content had more effect on increasing the strut thickness.

Interconnectivity. Another critical parameter in the performance of a scaffold is pore interconnectivity. All of the scaffolds investigated in the current study had interconnectivity greater than 99% by μCT analysis. With the complete salt removal, the only sources of porosity within the scaffold would be from salt leaching and trapped air pockets during the formulation. To assess the amount of trapped air or the packing efficiency of the resin−salt mixture, we carried out μCT image analysis on the polymer/salt composites prior to salt leaching, which showed that the overall void content did not exceed 0.2 vol %. The trapped air pocket in contact with the porogen would also lead to interconnected pores. The high degree of interconnectivity is expected since almost all pores result from the salt-leaching process, and leaching can only occur when extensive interconnectivity exists between the pores. While almost all pores are interconnected, the connectivity, which is a measure of the degree to which a solid structure is multiply connected, is different depending on the scaffold structure. The connectivity, calculated using a modified Euler's characteristic,[23] increased as the porogen sized decreased.

A truly interconnected scaffold would allow for the porogen to be quantitatively removed. Any residual salt would be undesirable and would potentially have a negative impact on the cell response. μCT was also useful in determining the presence of residual salt. Salt was quantitatively removed for all scaffolds except for the scaffold prepared with 70% (by mass) salt, which had minimal amount of residual salt (<0.05%). We also attempted to prepare scaffolds with 65% (by mass) salt in the initial formulation; however, these scaffolds did not yield interconnected structures as the majority of salt crystals remained trapped in the scaffolds even after 10 days of leaching in water. The current results show that interconnected scaffolds with

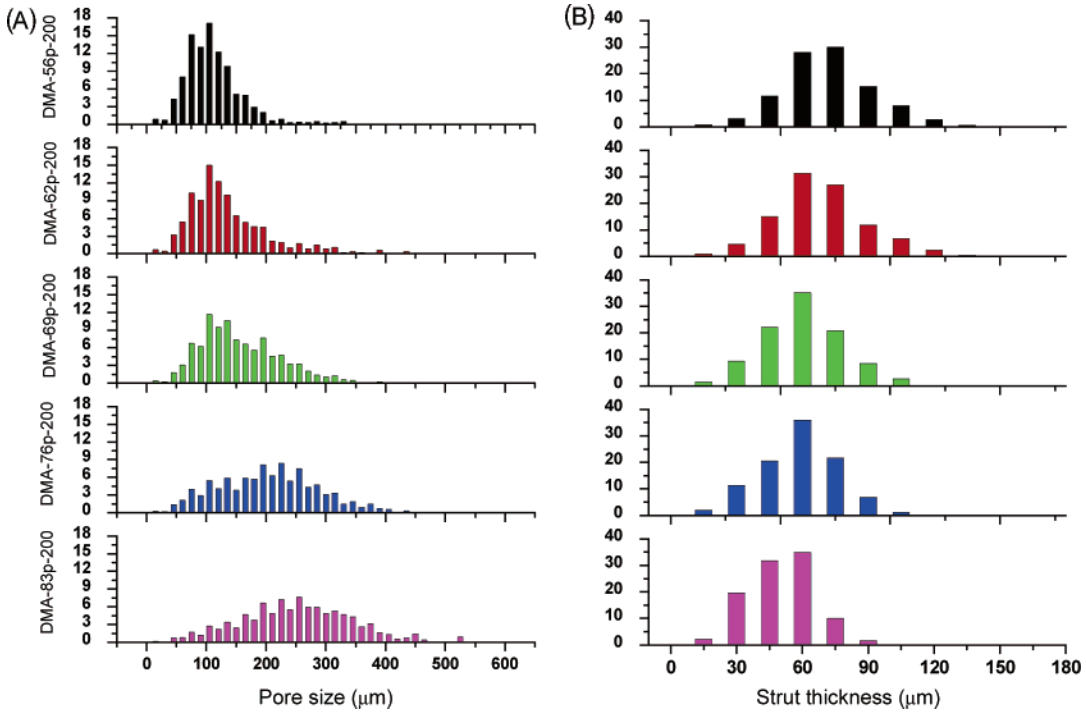

Figure 7. Analysis of (A) pore size and (B) strut thickness from the 3D μCT images of scaffolds prepared from 200-μm salt crystals with varying mass % of polymer.

porosities as low as 57% (by volume) can be prepared using 70% (by mass) initial salt content. This is significantly lower than a previous study which found that a lower limit of 80% (by mass) initial salt content was required to form interconnected structures.[8] The salt-leaching fabrication technique allows for a large range of scaffold porosities to be generated. The ability to form interconnected structures depends on not only the initial porogen content but also on the porogen size and size distribution. The present study demonstrates that the choice of porogen size greatly affects the morphometric parameters, specifically the ability to form fully interconnected scaffolds. In addition, the use of small porogen leads to smaller pores and greater connectivity.

Mechanical Properties. In this study, we have examined the compression moduli of the scaffolds as a function of the porous mesostructure. In compression, the stress−strain curves have a broadly similar shape exhibiting three distinct regions. At low stress and strain, the struts bend in a linear-elastic (recoverable) manner. Beyond a critical strain, the pores begin to collapse by mechanisms such as elastic buckling, plastic collapse, and brittle failure. Finally, compression densification of the scaffold causes a dramatic increase in the compression modulus at large strains. In our studies, relatively small strains were applied to the scaffold to determine the scaffold modulus comparing the relationship between scaffold structure and properties.

As shown in Figure 4, the strut thickness increased as the porogen size increased for the first series of scaffolds with a target porosity of 74%. By plotting the compression modulus as a function of average strut thickness (Figure 8a), it was observed that the modulus increased by a factor of 5 when the average strut thickness increased from approximately 25 to 75 μm for a fixed porosity. Results from the current study show a direct correlation between the compression modulus and strut thickness. At a constant porosity, an increase in the strut thickness is accompanied by a decrease in the number of struts. Our results indicate that the strut thickness, rather than the number of struts, is the predominate factor in determining the mechanical properties at a constant porosity. Since the strut thickness is directly related to the pore size, the mechanical properties increased with increased pore size. This is contrary to a previous study, which reported that the compressive modulus decreased as the pore size increased for sintered microsphere scaffolds with near constant porosities (35−40%).[17] The current scaffolds are connected by struts while sintered microsphere scaffolds are connected by the microsphere contact points. Because of differences in the architecture between our photopolymerized salt leached scaffolds and the sintered microsphere scaffolds, it is not surprising that different trends are observed; however, these findings illustrate the complexity and multitude of structural variables that affect the mechanical properties of a scaffold.

The compression moduli of the scaffolds prepared with varying polymer-to-salt ratios (series 2) are illustrated in Figure 8b. We achieved a range of moduli covering about 2 orders of magnitude for the composition range studied. Unlike the first series of scaffolds where the porosity was essentially constant, the porosity of the second series increased while the average wall thickness decreased as the polymer-to-salt ratio decreased. The net result is that both the strut thickness and the number of struts increase as the polymer content increased. For this series of scaffolds, the increase in average strut thickness was modest (from ca. 50 to 70 μm), but the porosity spanned a larger range. On the basis of the relationship between the strut thickness and compression modulus established in the first series of scaffolds, we expect the small change in the average strut thickness for the second series to have a limited effect on the compression modulus. Thus, the mechanical properties of the scaffold are governed primarily by the scaffold porosity. These results are consistent with trends observed for cancellous bone.[24]

The theories for foams with regular open- and closed-celled structures are well established and have been shown to agree well with experimental data.[13] For open-celled foams with regular structures, the relative Young's modulus (E^*/E_s) is related to the relative porosity ($1 - (r^*/r_s)$) by the following expression, $E^*/E_s = C(r^*/r_s)$,[2] where E^* and E_s are modulus of the foam and bulk solid material, respectively; r^* and r_s are the

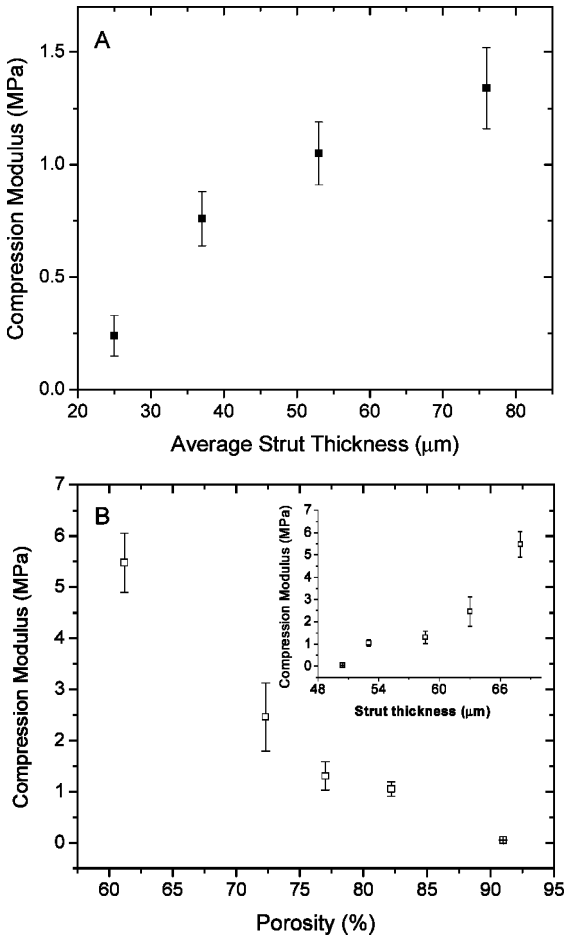

Figure 8. (A) Compression modulus of the DMA-74p scaffolds prepared with varying size porogens as a function of strut thickness from μCT analysis. (B) Porosity versus compression modulus, inset shows compression modulus as a function of strut size.

density of the foam and solid material, respectively; and C is a constant. The salt-leached scaffolds have pores and struts that are irregular in shape, and their dimensions have a broad size distribution. It is therefore no surprise that analysis of our data does not agree with this power law relationship. The mechanical properties of salt-leached scaffolds with irregular structures are significantly lower than that for the theoretical value calculated for structurally optimized foams. In addition, because of the irregular pore shapes and large distributions in dimensionality, we observed increased mechanical properties with the average strut thickness increased. Given the difficulties in predicting the mechanical properties of salt-leached scaffold, our results demonstrate the need to optimize the scaffold structure with respect to its mechanical performance. For salt-leached scaffolds, both the porosity and strut thickness affect the mechanical properties with porosity being the dominant factor. The scaffold with a porosity of 91% (Figure 8b) had a low compressive modulus; however, decreasing the porosity to 82% resulted in a 20-fold increase in modulus. Further decreases in porosity to 62% resulted in more modest improvements in modulus.

Conclusions

Detailed morphometric parameters and mechanical responses of tissue engineering scaffolds generated by the salt-leaching process are presented. Two strategies, varying the porogen size and varying the polymer-to-salt ratio, were used to control the scaffold structure. Morphometric parameters (e.g., porosity, pore size, strut thickness, and interconnectivity) were obtained using μCT, mercury porosimetry, and gravimetric analysis and were compared. For scaffolds prepared with the same polymer-to-salt ratio but different salt sizes, the porosity was relatively constant but both the average pore size and strut thickness increased as the salt size increased. An increase in compressive modulus was observed as the strut thickness increased. For scaffolds prepared with the same salt size but different polymer-to-salt ratios, the average strut thickness decreased while the average pore sizes increased as the polymer content decreased. When salt crystals with average size of 200 μm were used, interconnected scaffolds with broad porosity range (92−56%) could be prepared. Existing theories developed for foams did not accurately predict the mechanical properties of salt-leached scaffolds. Experimental results indicate that both the strut thickness and the porosity affect the mechanical properties, with the dominant contribution being the porosity. The current study demonstrates the interplay between various scaffold morphometric parameters and mechanical responses. The structure and properties of scaffolds can be adjusted on the basis of the choice of porogen and its size and size distribution.

Acknowledgment. The EBPADMA resins were kindly donated by Esstech, Inc. We would like to thank Dr. Cato T. Laurencin at the University of Virginia for allowing us to use the mercury porosimeter. In addition, the authors would like to thank Drs. Tithi Dutta Roy, Martin Y.M. Chiang, and Joy P. Dunkers for their advice and technical recommendations. Certain equipment, instruments, or materials are identified in this paper to adequately specify the experimental details. Such identification does not imply recommendation by the National Institute of Standards and Technology nor does it imply that the materials are necessarily the best available for the purpose. Official contribution of the National Institute of Standards and Technology; not subject to copyright in the United States.

References and Notes

(1) Hutmacher, D. W.; Sittinger, M.; Risbud, M. V. *Trends Biotechnol.* **2004**, *22*, 354−362.
(2) Yang, S. F.; Leong, K. F.; Du, Z. H.; Chua, C. K. *Tissue Eng.* **2002**, *8*, 1−11.
(3) Yang, S. F.; Leong, K. F.; Du, Z. H.; Chua, C. K. *Tissue Eng.* **2001**, *7*, 679−689.
(4) Quirk, R. A.; France, R. M.; Shakesheff, K. M.; Howdle, S. M. *Curr. Opin. Solid State Mater. Sci.* **2004**, *8*, 313−321.
(5) Karageorgiou, V.; Kaplan, D. *Biomaterials* **2005**, *26*, 5474−5491.
(6) Fisher, J. P.; Dean, D.; Engel, P. S.; Mikos, A. G. *Annu. Rev. Mater. Res.* **2001**, *31*, 171−181.
(7) Landis, F. A.; Stephens, J. S.; Cooper, J. A.; Cicerone, M. T.; Lin-Gibson, S. *Biomacromolecules* **2006**, *7*, 1751−1757.
(8) Fisher, J. P.; Holland, T. A.; Dean, D.; Engel, P. S.; Mikos, A. G. *J. Biomater. Sci., Polym. Ed.* **2001**, *12*, 673−687.
(9) Wang, S. F.; Lu, L. C.; Yaszemski, M. J. *Biomacromolecules* **2006**, *7*, 1976−1982.
(10) Ho, S. T.; Hutmacher, D. W. *Biomaterials* **2006**, *27*, 1362−1376.
(11) Moore, M. J.; Jabbari, E.; Ritman, E. L.; Lu, L. C.; Currier, B. L.; Windebank, A. J.; Yaszemski, M. J. *J. Biomed. Mater. Res., Part A* **2004**, *71A*, 258−267.
(12) Karande, T. S.; Ong, J. L.; Agrawal, C. M. *Ann. Biomed. Eng.* **2004**, *32*, 1728−1743.
(13) Gibson, L. J.; Ashby, M. F. *Cellular Solids: Structure and Properties;* 2nd ed.; Cambridge University Press: Cambridge, U.K., 1997.
(14) Lin, A. S. P.; Barrows, T. H.; Cartmell, S. H.; Guldberg, R. E. *Biomaterials* **2003**, *24*, 481−489.
(15) Barralet, J. E.; Grover, L.; Gaunt, T.; Wright, A. J.; Gibson, I. R. *Biomaterials* **2002**, *23*, 3063−3072.
(16) Barralet, J. E.; Gaunt, T.; Wright, A. J.; Gibson, I. R.; Knowles, J. C. *J. Biomed. Mater. Res.* **2002**, *63*, 1−9.

(17) Borden, M.; El-Amin, S. F.; Attawia, M.; Laurencin, C. T. *Biomaterials* **2003**, *24*, 597−609.
(18) Woodfield, T. B. F.; Malda, J.; de Wijn, J.; Peters, F.; Riesle, J.; van Blitterswijk, C. A. *Biomaterials* **2004**, *25*, 4149−4161.
(19) Hildebrand, T.; Ruegsegger, P. *J. Microsc. (Oxford)***1997**, *185*, 67−75.
(20) Giesche, H. *Part. Part. Syst. Charact.* **2006**, *23*, 9−19.
(21) *ASTM Book of Standards;* Vol 08.01. D 1621-04a, 2004.
(22) Gupta, N. Kishore; Woldesenbet, E.; Sankaran, S. *J. Mater. Sci.* **2001**, *36*, 4485−4491.
(23) Odgaard, A.; Gundersen, H. J. G. *Bone* **1993**, *14*, 173−182.
(24) Kabel, J.; Odgaard, A.; van Rietbergen, B.; Huiskes, R. *Bone* **1999**, *24*, 115−120.

BM061139Q